ELSEVIER

International Journal of Solids and Structures 41 (2004) 4517–4533

INTERNATIONAL JOURNAL OF SOLIDS and STRUCTURES

www.elsevier.com/locate/ijsolstr

Bistable composite slit tubes. I. A beam model

Diana A. Galletly, Simon D. Guest *

Department of Engineering, University of Cambridge, Trumpington Street, Cambridge CB2 1PZ, UK

Received 23 September 2003; received in revised form 13 February 2004
Available online 15 April 2004

Abstract

Composite slit tubes with a circular cross-section show an interesting variety in their large-deformation behaviour, that depends on the layup of the surface that is used: tubes made from many antisymmetric laminae are bistable, and have a compact coiled configuration, tubes made from similar, but symmetric, laminae do not have a compact coiled state, and indeed may not be bistable, while tubes made from an isotropic sheet are not bistable. A simple model is presented here that is able to distinguish between these behaviours; it assumes that the cross-section remains circular, but allows twist, which is shown to be the key to making the distinction between the behaviours described.

Keywords: Bistable; Composite

1. Introduction

The composite slit tubes described here are straight, thin-walled ribs with a cross-section that is a circular arc. When made from particular layups of composite, these structures have two stable states: an extended state where there is transverse curvature but no longitudinal curvature, and a coiled state where there is longitudinal curvature and minimal transverse curvature; an example structure is shown in Fig. 1.

The bistable behaviour shown in Fig. 1 is not only a function of the geometry of the structure, but also of the bending and in-plane stiffness of the surface. Structures with similar geometry, but made from an isotropic metal sheet, are known as tape-springs (Seffen and Pellegrino, 1999), or STEM's (Rimrott, 1966): STEM's do not exhibit bistability, and require a spindle or casing to hold them when coiled. The bistable structure shown in Fig. 1 is made from a laminate where the plies are *antisymmetric* with respect to the mid-surface. If the structure was made from a more conventional *symmetric* layup, the structure may not be bistable, and attempting to coil it results in the structure taking up a helical shape. This paper will describe a model that is able to reproduce these behaviours.

Previously Iqbal et al. (2000) described a simple theoretical model for bistable composite slit tubes which calculates the total strain energy of the shell as a function of the transverse and longitudinal curvatures, and

* Corresponding author. Tel.: +44-1223-332708; fax: +44-1223-332662.
E-mail addresses: dag1000@eng.cam.ac.uk (D.A. Galletly), sdg@eng.cam.ac.uk (S.D. Guest).

0020-7683/$ - see front matter © 2004 Elsevier Ltd. All rights reserved.
doi:10.1016/j.ijsolstr.2004.02.036

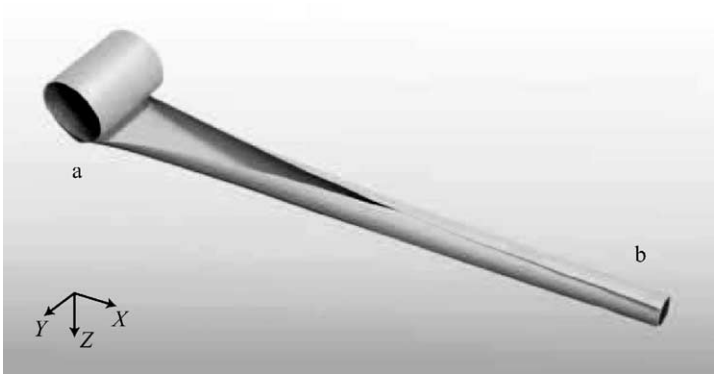

Fig. 1. A bistable composite slit tube: (a) coiled and (b) extended. This paper will not consider the transition between (a) and (b) shown, but will assume that the entire tube is either coiled or extended. The global coordinate system X, Y, Z used in the beam model is shown.

the angle subtended by the cross-section of the shell. This model provides an excellent insight into the behaviour of the bistable structures, and gives a good prediction of the behaviour of strips with a simple antisymmetric layup. However, because it restricts possible modes of deformation, it is not able to distinguish between the behaviour exhibited by symmetric laminates, antisymmetric laminates, and isotropic systems.

This paper, together with a companion paper, Part II (Galletly and Guest, 2004) describe more comprehensive analytical models for composite slit tubes. One basic assumption, unchanged from Iqbal et al. (2000), is that the structures are longitudinally uniform, and thus the models are making no attempt to model the transition from the rolled to the extended state, which takes place in a transition zone that can be seen in Fig. 1. The models are instead trying to give information about the two possible stable shapes. Within the assumption of longitudinal uniformity, this paper allows the structure to take any shape longitudinally, whilst assuming that the cross-section remains as an arc of a circle, with a radius that is allowed to vary. Part II will, in addition, allow any cross-sectional shape.

One important assumption that is made both here and in Part II is that the tubes are initially unstressed, and hence we are not considering the behaviour of prestressed systems such as those recently described by Kebadze et al. (in press). However, it would be straightforward to incorporate the effect of prestress into the models described here.

The paper is structured as follows. Section 2 will describe the beam model, including its key innovation, that it allows the tubes to twist. Section 3 presents the results of applying this model to four sample tubes: one is made from an antisymmetric laminate; two are made from symmetric laminae; and one is made from an isotropic sheet. Section 4 presents a brief comparison with previous experiments and computations, and Section 5 concludes the paper.

2. Derivation of model

It is assumed that the tube is initially unstrained in its extended state, as shown in Fig. 2. The tube geometry is defined by two length parameters, the width l, and the initial radius of curvature R; it is assumed to be infinitely long. To fully define the tube also requires the in-plane and bending stiffness properties of the shell to be defined; these are described in Section 2.3.

The beam model, described here, assumes that the beam deforms while remaining longitudinally uniform, with a cross-section that is an arc of a circle who's radius may change. Its configuration is then fully defined by four *global strain parameters* which will be described next, in Section 2.1. Section 2.2 describes

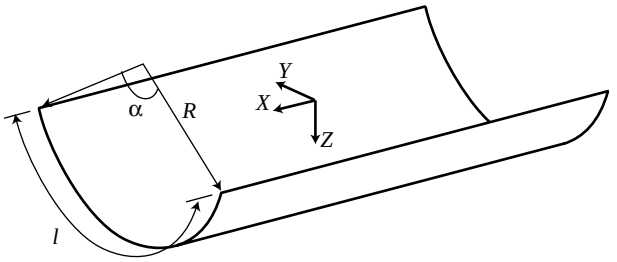

Fig. 2. The initial geometric parameters for the bistable tube, R and l, and the global coordinate system used for describing deformations and loads. The X-axis is in the longitudinal direction, and the Y-axis is in the transverse direction. The angle $\alpha = l/R$ will be used for presenting results in Section 3.

the kinematic relationships between these global strain parameters, and local strains in the shell, and Section 2.3 describes the stress–strain relationship between these strains and the corresponding local stresses. Section 2.4 integrates these stresses to give global forces, work-conjugate to the global strain parameters: setting these forces to zero gives equilibrium configurations of the structure, and Section 2.5 describes the stability calculations for these configurations.

2.1. Global strain parameters

The assumption that the structure is uniform longitudinally allows six *beam deformation* modes: extension, E_X; twist, Φ_X; bending about two axes, K_Y and K_Z; and two shear modes, Γ_{XY} and Γ_{XZ}. These modes are shown in Fig. 3.

In fact, the beam model considers only three of the beam deformation modes shown in Fig. 3. Two we can exclude by symmetry: the system has a twofold rotational symmetry about the Z-axis, and E_X, K_Y, Φ_X and Γ_{XY} are preserved by this symmetry operation, while K_Z and Γ_{XZ} are reversed. Thus, K_Z and Γ_{XZ} would only be of interest through some symmetry-breaking phenomenon that is not observed in experiments, and hence K_Z and Γ_{XZ} are assumed to be zero. We also exclude the shear modes, Γ_{XY} and Γ_{XZ} because we do not wish to explicitly constrain *warping*, and the deformations corresponding to Γ_{XY} and Γ_{XZ} are simply warping of the cross-section.

Thus the beam model considers three beam deformation modes, E_X, K_Y, Φ_X, to which we add a further parameter to describe the transverse curvature of the section, K_T. Our model therefore describes the configuration of the slit tube by four parameters. In the initial state $E_X = K_Y = \Phi_X = 0$, and $K_T = 1/R$, and this is the first equilibrium point. These four global strain parameters fully define the shape of the structure; next we will consider the deformations of the surface, the *local strains*, that result from varying these four parameters.

2.2. Local strains

Changing the global strain parameters from the initial values causes deformation of the structure. This section considers the structure as a shell, and derives expressions for the strains due to changes in the global strain parameters. The strains in the structure vary with position in the cross-section, described by the parameter s, shown in Fig. 4; they are described in a local coordinate system $x(s)$, $y(s)$, $z(s)$. At the centre of the structure, these axes are aligned with the global system, but off-centre the z-axis remains perpendicular, and the y-axis parallel, to the surface.

To describe the deformation of a shell generally requires six generalised strain parameters. However, we only consider four of these, extension in the x-direction, ϵ_x, curvature in the x- and y-directions, κ_x and κ_y,

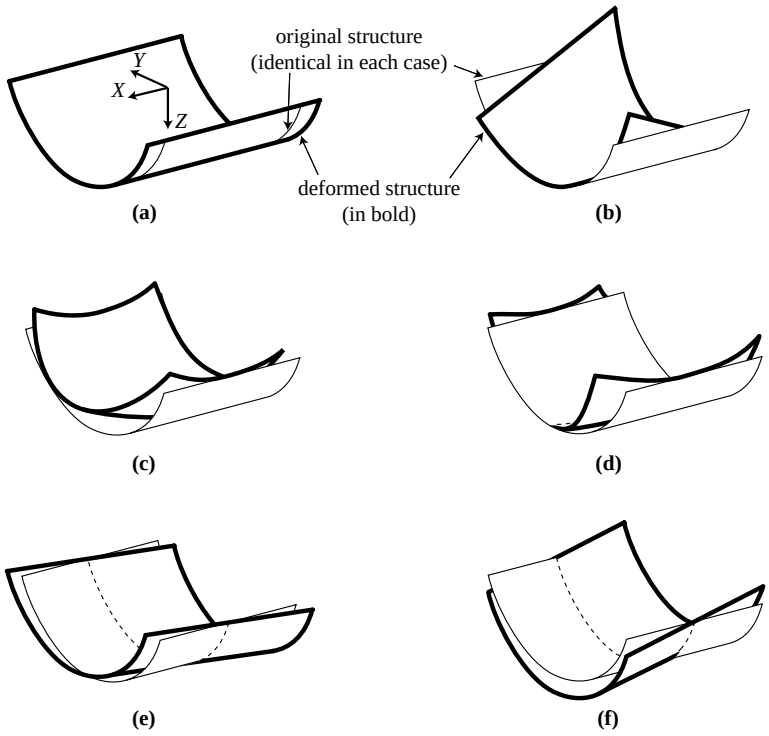

Fig. 3. Six *beam deformation* modes: (a) extension, E_X; (b) twist, Φ_X; (c) bending K_Y; (d) bending K_Z; (e) shear Γ_{XY}; (f) shear, Γ_{XZ}. Only E_X, Φ_X and K_Y are allowed in the beam model for the bistable tube.

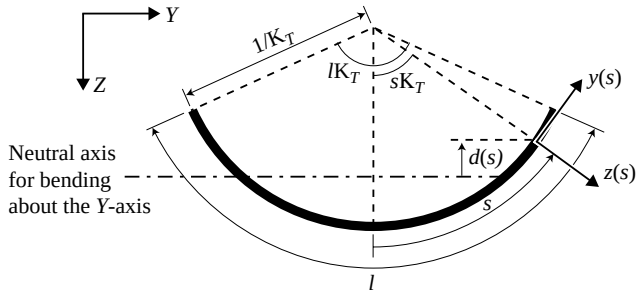

Fig. 4. A cross section of the beam.

and curvature of the surface, κ_{xy}. Extension transversely, ϵ_y, and shear, γ_{xy}, are not defined by the global deformation modes, and we assume that these are not explicitly constrained. That shear deformation is allowed is consistent with our assumption in Section 2.1 that the surface is allowed to warp.

Note our convention that global strains of the system, considered as a beam, are denoted using upper-case letters, while local strains of the surface, considered as a shell, are denoted using lower-case letters. It is also worth noting here that treating the structure as both a beam and a shell leads to potential confusion because of the differing standard notations for curvature. As a beam, where the X-axis defines the longitudinal direction, K_Y describes the rotation of the cross-section around the Y-axis as one moves along the

beam. As a shell, where the z-axis describes a normal to the surface, κ_x describes a similar rotation of the surface around the y-axis as one moves in the x-direction. Thus along the centre-line of the beam, where x, y, z and X, Y, Z coincide, $\kappa_x = K_Y$.

2.2.1. Strains due to twisting

The strains due to twisting are the most complex part of this exposition, and hence are detailed separately.

We make the assumption that due to twisting, each section rotates about the centre-line of the structure; choice of rotation axis does not affect the resultant local twist of the surface (Timoshenko and Gere, 1961, Chapter 5) but does affect the longitudinal extension. An alternative, more difficult, assumption, would be that each section rotates about its shear centre. However, for small K_T the expressions reduce to the same values, which will be described in Section 2.2.5.

We note here the convention that we will use for twist of the surface, κ_{xy}. Literature on shell and plate theory, and on composite theory, use different conventions (similar to the distinction between engineering and mathematical shear strain). We shall use the composite theory definition, $\kappa_{xy} = -2\partial^2 w/\partial x\,\partial y$, where w is the displacement of the surface in the out-of-plane, z, direction, as defined by Halpin (1984) (the literature on shell and plate theory would define κ_{xy} to be half this value).

Consider the small section of surface shown in Fig. 5. The rotation of a cross-section at a distance x from a reference section is given by $\theta = \Phi_X x$, and the displacement in the z-direction of a point at (x, y) is given by $w = \theta y = \Phi_X xy$. Thus

$$\Phi_X = \frac{\partial^2 w}{\partial x\,\partial y}, \tag{1}$$

and κ_{xy} is given by

$$\kappa_{xy} = -2\frac{\partial^2 w}{\partial x\,\partial y} = -2\Phi_X. \tag{2}$$

The global twist mode, Φ_X, will cause longitudinal fibres to take up a helical shape, and hence also cause some extension. A longitudinal fibre at a distance c from the axis of rotation will end up at an orientation $c\Phi_X$ to the longitudinal axis. A short length of fibre is shown in Fig. 6, and will (neglecting higher-order terms), undergo a strain ϵ,

$$\epsilon = \frac{\Phi_X^2 c^2}{2}. \tag{3}$$

The length c, as shown in Fig. 7 is given by

$$c = \frac{2}{K_T}\sin\left(\frac{sK_T}{2}\right), \tag{4}$$

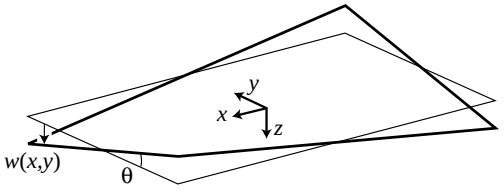

Fig. 5. A small section of twisted surface.

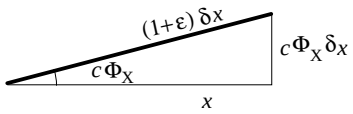

Fig. 6. A short length of twisted longitudinal fibre.

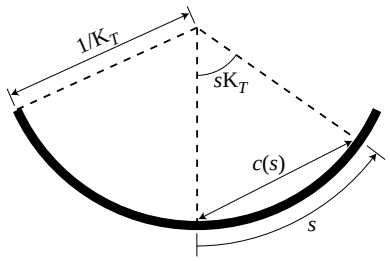

Fig. 7. A cross-section of the beam, showing the distance from the central fibre.

and hence

$$\epsilon = \frac{2\Phi_X^2}{K_T^2}\sin^2\left(\frac{sK_T}{2}\right). \tag{5}$$

2.2.2. Longitudinal strain

Beam extension, beam bending, and beam twisting (Eq. (5)) will cause longitudinal strain:

$$\epsilon_x(s) = E_X - d(s)K_Y + \frac{2\Phi_X^2}{K_T^2}\sin^2\left(\frac{sK_T}{2}\right), \tag{6}$$

where $d(s)$ is the distance from the neutral axis for bending about the Y-axis, as shown in Fig. 4.

Geometry shows that $d(s)$ is given by

$$d(s) = \frac{1}{K_T}\left[\frac{2}{lK_T}\sin\frac{lK_T}{2} - \cos sK_T\right], \tag{7}$$

and hence

$$\epsilon_x(s) = E_X - \frac{K_Y}{K_T}\left[\frac{2}{lK_T}\sin\frac{lK_T}{2} - \cos sK_T\right] + \frac{2\Phi_X^2}{K_T^2}\sin^2\left(\frac{sK_T}{2}\right). \tag{8}$$

2.2.3. Longitudinal curvature

A component of beam curvature will cause local longitudinal curvature,

$$\kappa_x(s) = K_Y\cos sK_T. \tag{9}$$

The angle sK_T is shown in Fig. 4.

2.2.4. Transverse curvature

κ_y is equal to the change in the transverse curvature, K_T, from its initial value $1/R$:

$$\kappa_y = K_T - \frac{1}{R}. \tag{10}$$

2.2.5. Kinematic relationships for small cross-sectional curvature

Experience with using the model described here shows that the interesting behaviour occurs when the cross-sectional curvature is small, which allows the expressions derived to be simplified. Here we present simplified equations for the local strains that will be used in later calculations, found from Eqs. (8)–(10) and (2) by assuming that K_T is small, and neglecting K_T^2, and higher powers:

$$\epsilon_x = E_X + \frac{K_Y K_T}{2}\left[\frac{l^2}{12} - s^2\right] + \frac{\Phi_X^2 s^2}{2}, \tag{11}$$

$$\kappa_x = K_Y, \tag{12}$$

$$\kappa_y = K_T - \frac{1}{R}, \tag{13}$$

$$\kappa_{xy} = -2\Phi_X. \tag{14}$$

2.3. Stress–strain relationship

Although the deflections in the structure are large, we assume that the strains remain small, and the general, linear stress–strain relationship for a composite material is then given by

$$\begin{pmatrix} N_x \\ N_y \\ N_{xy} \\ - \\ M_x \\ M_y \\ M_{xy} \end{pmatrix} = \left[\begin{array}{ccc|ccc} A_{11} & A_{12} & A_{16} & B_{11} & B_{12} & B_{16} \\ A_{12} & A_{22} & A_{26} & B_{12} & B_{22} & B_{26} \\ A_{16} & A_{26} & A_{66} & B_{16} & B_{26} & B_{66} \\ - & - & - & - & - & - \\ B_{11} & B_{12} & B_{16} & D_{11} & D_{12} & D_{16} \\ B_{12} & B_{22} & B_{26} & D_{12} & D_{22} & D_{26} \\ B_{16} & B_{26} & B_{66} & D_{16} & D_{26} & D_{66} \end{array}\right] \begin{pmatrix} \epsilon_x \\ \epsilon_y \\ \gamma_{xy} \\ - \\ \kappa_x \\ \kappa_y \\ \kappa_{xy} \end{pmatrix}, \tag{15}$$

where ϵ_x, ϵ_y, γ_{xy}, κ_x, κ_y and κ_{xy} are the generalised strains, already introduced, and N_x, N_y, N_{xy}, M_x, M_y and M_{xy} are the corresponding stress resultants. The A_{ij} are the *laminate extensional stiffnesses*, relating extensional and shear forces to extensional and shear strains. The B_{ij} are the *laminate coupling stiffnesses*, relating extensional and shear forces to bending and twisting curvatures, and bending and twisting moments to extensional and shear strains. The D_{ij} are the *laminate bending stiffnesses*, relating bending and twisting moments to bending and twisting curvatures. The theory explaining how these laminate stiffnesses are calculated can be found in any good primer on composite materials, for example Hull (1981) or Halpin (1984).

In this model, no forces are applied at the edges of the tube. Hence $N_y = N_{xy} = 0$ here, and we assume that this is true throughout the tube; correspondingly, we take ϵ_y and γ_{xy} to be unconstrained. We can rewrite Eq. (15) as

$$\begin{pmatrix} N_x \\ M_x \\ M_y \\ M_{xy} \\ - \\ 0 \\ 0 \end{pmatrix} = \left[\begin{array}{cccc|cc} A_{11} & B_{11} & B_{12} & B_{16} & A_{12} & A_{16} \\ B_{11} & D_{11} & D_{12} & D_{16} & B_{12} & B_{16} \\ B_{12} & D_{12} & D_{22} & D_{26} & B_{22} & B_{26} \\ B_{16} & D_{16} & D_{26} & D_{66} & B_{26} & B_{66} \\ - & - & - & - & - & - \\ A_{12} & B_{12} & B_{22} & B_{26} & A_{22} & A_{26} \\ A_{16} & B_{16} & B_{26} & B_{66} & A_{26} & A_{66} \end{array}\right] \begin{pmatrix} \epsilon_x \\ \kappa_x \\ \kappa_y \\ \kappa_{xy} \\ - \\ \epsilon_y \\ \gamma_{xy} \end{pmatrix}. \tag{16}$$

Thus we find that ϵ_y and γ_{xy} are given by

$$\begin{pmatrix} \epsilon_y \\ \gamma_{xy} \end{pmatrix} = -\begin{bmatrix} A_{22} & A_{26} \\ A_{26} & A_{66} \end{bmatrix}^{-1} \begin{bmatrix} A_{12} & B_{12} & B_{22} & B_{26} \\ A_{16} & B_{16} & B_{26} & B_{66} \end{bmatrix} \begin{pmatrix} \epsilon_x \\ \kappa_x \\ \kappa_y \\ \kappa_{xy} \end{pmatrix}, \tag{17}$$

and the remaining stress resultants are given by

$$\begin{pmatrix} N_x \\ M_x \\ M_y \\ M_{xy} \end{pmatrix} = \begin{bmatrix} A^*_{11} & B^*_{11} & B^*_{12} & B^*_{16} \\ B^*_{11} & D^*_{11} & D^*_{12} & D^*_{16} \\ B^*_{12} & D^*_{12} & D^*_{22} & D^*_{26} \\ B^*_{16} & D^*_{16} & D^*_{26} & D^*_{66} \end{bmatrix} \begin{pmatrix} \epsilon_x \\ \kappa_x \\ \kappa_y \\ \kappa_{xy} \end{pmatrix}, \tag{18}$$

which we write as $\underline{N} = [\mathbf{K}^*]\underline{\epsilon}$, where the *reduced* stiffness matrix $[\mathbf{K}^*]$ is given by

$$[\mathbf{K}^*] = \left(\begin{bmatrix} A_{11} & B_{11} & B_{12} & B_{16} \\ B_{11} & D_{11} & D_{12} & D_{16} \\ B_{12} & D_{12} & D_{22} & D_{26} \\ B_{16} & D_{16} & D_{26} & D_{66} \end{bmatrix} - \begin{bmatrix} A_{12} & A_{16} \\ B_{12} & B_{16} \\ B_{22} & B_{26} \\ B_{26} & B_{66} \end{bmatrix} \begin{bmatrix} A_{22} & A_{26} \\ A_{26} & A_{66} \end{bmatrix}^{-1} \begin{bmatrix} A_{12} & B_{12} & B_{22} & B_{26} \\ A_{16} & B_{16} & B_{26} & B_{66} \end{bmatrix} \right). \tag{19}$$

For any antisymmetric layup, symmetry arguments show that $B^*_{11} = B^*_{12} = D^*_{16} = D^*_{26} = 0$. Similarly, for a symmetric layup, $B^*_{11} = B^*_{12} = B^*_{16} = 0$. The systems in this paper will all either be antisymmetric, or symmetric, and $B^*_{11} = B^*_{12} = 0$ will be used to simplify the algebra in the next section.

2.4. Derivation of global forces

Corresponding in a work sense to each of the global strain parameters, E_X, K_Y, Φ_X, K_T will be a *global force*: a tension P, a longitudinal moment M_L, a torque T and a transverse moment/unit length, M_T. To find an equilibrium position, we are looking for a position where each of these equals zero.

2.4.1. Global tension

The global tension is given by

$$P = \int_{-\frac{l}{2}}^{\frac{l}{2}} N_x \, \mathrm{d}s. \tag{20}$$

For the symmetric and antisymmetric sections that we are considering, from Eq. (18) with $B^*_{11} = B^*_{12} = 0$,

$$N_x = A^*_{11}\epsilon_x + B^*_{16}\kappa_{xy}, \tag{21}$$

and substituting from the kinematic relationships Eqs. (11) and (14),

$$N_x = A^*_{11}\left(E_X + \frac{K_Y K_T}{2}\left[\frac{l^2}{12} - s^2\right] + \frac{\Phi_X^2 s^2}{2} \right) - 2B^*_{16}\Phi_X. \tag{22}$$

Thus, completing the integration

$$P = A^*_{11}\left(E_X l + \frac{\Phi_X^2 l^3}{24} \right) - 2B^*_{16}\Phi_X l. \tag{23}$$

As will be seen later, the global strain E_X only occurs in the expression for this global force, and not any other. Thus, it is straightforward to ensure that $P = 0$ by finding an expression for E_X and substituting this algebraically into the other kinematic relationships.

Setting $P = 0$ gives

$$E_X = 2\frac{B^*_{16}}{A^*_{11}}\Phi_X - \frac{\Phi_X^2 l^2}{24}, \tag{24}$$

and substituting into expressions for the strains, Eqs. (11)–(14) gives

$$\epsilon_x = \frac{K_Y K_T}{2}\left[\frac{l^2}{12} - s^2\right] + \frac{\Phi_X^2}{2}\left[s^2 - \frac{l^2}{12}\right] + 2\frac{B^*_{16}}{A^*_{11}}\Phi_X, \tag{25}$$

$$\kappa_x = K_Y, \tag{26}$$

$$\kappa_y = K_T - \frac{1}{R}, \tag{27}$$

$$\kappa_{xy} = -2\Phi_X. \tag{28}$$

These expressions, functions of only K_Y, K_T and Φ_X, will be used for calculating the other global forces.

2.4.2. Global torque

It was clear how to find the global tension in the beam, but the relationships are not so simple for the three remaining global forces. We shall calculate these using Virtual Work.

To calculate the torque, we consider that if a small change in the twist $\delta\Phi^*_X$ occurs, the internal work done must be equal to the external work. The external work per unit length is given by $T\,\delta\Phi^*_X$. To calculate the internal work, we must first calculate the changes in the strains which are compatible with $\delta\Phi^*_X$:

$$\underline{\delta\epsilon} = \frac{\partial \underline{\epsilon}}{\partial \Phi_X}\delta\Phi^*_X, \tag{29}$$

where $\underline{\epsilon}$ is the initial strain vector, and $\underline{\delta\epsilon}$ is the vector of strain increments. The internal work done per unit length is thus given by

$$W = \int_{-\frac{l}{2}}^{\frac{l}{2}} \underline{\delta\epsilon}^{\mathrm{T}} \cdot \underline{N}\,\mathrm{d}s = \int_{-\frac{l}{2}}^{\frac{l}{2}} \delta\Phi^*_X \frac{\partial \underline{\epsilon}}{\partial \Phi_X} \cdot \underline{N}\,\mathrm{d}s, \tag{30}$$

where $\underline{N}$ is the vector of internal forces. Equating the internal and external work, and cancelling both sides by $\delta\Phi^*_X$ we find an expression for the torque:

$$T = \int_{-\frac{l}{2}}^{\frac{l}{2}} \frac{\partial \underline{\epsilon}}{\partial \Phi_X} \cdot \underline{N}\,\mathrm{d}s. \tag{31}$$

Expanding this out gives

$$T = \int_{-\frac{l}{2}}^{\frac{l}{2}} \left(N_x \frac{\partial \epsilon_x}{\partial \Phi_X} + M_x \frac{\partial \kappa_x}{\partial \Phi_X} + M_y \frac{\partial \kappa_y}{\partial \Phi_X} + M_{xy} \frac{\partial \kappa_{xy}}{\partial \Phi_X}\right)\mathrm{d}s. \tag{32}$$

As $\partial\kappa_x/\partial\Phi_X = \partial\kappa_y/\partial\Phi_X = 0$ this simplifies to

$$T = \int_{-\frac{l}{2}}^{\frac{l}{2}} \left(N_x \frac{\partial \epsilon_x}{\partial \Phi_X} + M_{xy} \frac{\partial \kappa_{xy}}{\partial \Phi_X}\right)\mathrm{d}s. \tag{33}$$

After substituting for these terms, and integrating with respect to s, we obtain the following:

$$T = A^*_{11}\left[\left(\Phi_X^2 - K_Y K_T\right)\frac{\Phi_X l^5}{360}\right] - 2D^*_{16} l K_Y - 2D^*_{26} l\left(K_T - \frac{1}{R}\right) + 4\left(D^*_{66} - \frac{B^{*2}_{16}}{A^*_{11}}\right) l\Phi_X. \tag{34}$$

2.4.3. Global longitudinal moment

A virtual work approach shows that the longitudinal moment, M_l is given by

$$M_l = \int_{-\frac{l}{2}}^{\frac{l}{2}} \left(N_x \frac{\partial \epsilon_x}{\partial K_Y} + M_x \frac{\partial \kappa_x}{\partial K_Y} + M_y \frac{\partial \kappa_y}{\partial K_Y} + M_{xy} \frac{\partial \kappa_{xy}}{\partial K_Y} \right) \mathrm{d}s. \tag{35}$$

As $\partial \kappa_y / \partial K_Y = \partial \kappa_{xy} / \partial K_Y = 0$ this simplifies to

$$M_l = \int_{-\frac{l}{2}}^{\frac{l}{2}} \left(N_x \frac{\partial \epsilon_x}{\partial K_Y} + M_x \frac{\partial \kappa_x}{\partial K_Y} \right) \mathrm{d}s. \tag{36}$$

After substituting for these terms, and integrating with respect to s, we obtain the following:

$$M_l = A_{11}^* \left[\left(K_Y K_T - \Phi_X^2 \right) \frac{K_T l^5}{720} \right] + D_{11}^* l K_Y + D_{12}^* l \left(K_T - \frac{1}{R} \right) - 2 D_{16}^* l \Phi_X. \tag{37}$$

2.4.4. Global transverse moment

A virtual work approach shows that the transverse moment, M_T is given by

$$M_T = \int_{-\frac{l}{2}}^{\frac{l}{2}} \left(N_x \frac{\partial \epsilon_x}{\partial K_T} + M_x \frac{\partial \kappa_x}{\partial K_T} + M_y \frac{\partial \kappa_y}{\partial K_T} + M_{xy} \frac{\partial \kappa_{xy}}{\partial K_T} \right) \mathrm{d}s. \tag{38}$$

As $\partial \kappa_x / \partial K_T = \partial \kappa_{xy} / \partial K_T = 0$ this simplifies to

$$M_T = \int_{-\frac{l}{2}}^{\frac{l}{2}} \left(N_x \frac{\partial \epsilon_x}{\partial K_T} + M_y \frac{\partial \kappa_y}{\partial K_T} \right) \mathrm{d}s. \tag{39}$$

After substituting for these terms, and integrating with respect to s, we obtain the following:

$$M_T = A_{11}^* \left[\left(K_Y K_T - \Phi_X^2 \right) \frac{K_Y l^5}{720} \right] + D_{12}^* l K_Y + D_{22}^* l \left(K_T - \frac{1}{R} \right) - 2 D_{26}^* l \Phi_X. \tag{40}$$

2.5. Stability criteria

Finding an equilibrium point requires that $T = M_l = M_T = 0$, but it is also necessary to know about the stability of this equilibrium. This can be determined by examining the local tangent-stiffness matrix, [**H**], given in Eq. (41). If [**H**] is positive-definite, the equilibrium will be stable; the test for positive-definiteness used in this paper is that the smallest eigenvalue of [**H**], the stiffness of the softest mode of deformation, must be positive:

$$[\mathbf{H}] = \begin{bmatrix} \frac{\partial T}{\partial \Phi_X} & \frac{\partial M_l}{\partial \Phi_X} & \frac{\partial M_T}{\partial \Phi_X} \\ \frac{\partial T}{\partial K_Y} & \frac{\partial M_l}{\partial K_Y} & \frac{\partial M_T}{\partial K_Y} \\ \frac{\partial T}{\partial K_T} & \frac{\partial M_l}{\partial K_T} & \frac{\partial M_T}{\partial K_T} \end{bmatrix}, \tag{41}$$

where,

$$\begin{aligned}
\frac{\partial T}{\partial \Phi_X} &= A_{11}^* \left[\left(3\Phi_X^2 - K_Y K_T\right) \frac{l^5}{360} \right] + 4\left(D_{66}^* - \frac{B_{16}^{*2}}{A_{11}^*} \right) l, \\
\frac{\partial M_l}{\partial \Phi_X} &= -A_{11}^* \Phi_X \frac{K_T l^5}{360} - 2D_{16}^* l, \\
\frac{\partial M_T}{\partial \Phi_X} &= -A_{11}^* \Phi_X \frac{K_Y l^5}{360} - 2D_{26}^* l, \\
\frac{\partial M_T}{\partial K_T} &= A_{11}^* \frac{K_Y^2 l^5}{720} + D_{22}^* l, \\
\frac{\partial M_l}{\partial K_T} &= A_{11}^* \left[\left(2K_Y K_T - \Phi_X^2\right) \frac{l^5}{720} \right] + D_{12}^* l, \\
\frac{\partial M_l}{\partial K_Y} &= A_{11}^* \frac{K_T^2 l^5}{720} + D_{11}^* l.
\end{aligned} \tag{42}$$

The matrix [**H**] is, of course, symmetric: $\partial T/\partial K_Y = \partial M_l/\partial \Phi_X$, $\partial T/\partial K_T = \partial M_T/\partial \Phi_X$ and $\partial M_T/\partial K_Y = \partial M_l/\partial K_T$.

3. Results

Results are presented for four sample cases which are chosen to show the range of possible behaviours for these systems, and to allow some comparison with previously published experimental results, in Section 4. For each case we show:

- simplified expressions for the torque and moments, taking into account the appropriate zero terms in the reduced stiffness matrix;
- the reduced stiffness matrix;
- the position of equilibrium points other than the original, for varying α (shown in Fig. 2), and whether these equilibria are stable.

The results are presented for three tubes made from different laminae, and one tube made from an isotropic sheet. The laminate results presented are for 5-layer laminates; each ply is 0.21 mm thick, with a polypropylene matrix containing 30% volume fraction of glass fibres. One antisymmetric laminate is chosen that has been studied previously, both experimentally and computationally; the layers are laid up with the glass at $[+45°, -45°, 0°, +45°, -45°]$ to the longitudinal direction. A similar symmetric laminate is also presented with the glass at $[+45°, -45°, 0°, -45°, +45°]$ to the longitudinal direction. This proves not to have a second stable state for practical systems, and hence a second symmetric laminate is presented that does have a second stable state, where the layup is $[+40°, -40°, 0°, -40°, +40°]$. The isotropic results are presented for a 0.125 mm thick steel sheet. Further details of the materials will be found in Galletly (2001).

3.1. Antisymmetric layup

For an antisymmetric layup, where $D_{16}^* = D_{26}^* = 0$, the expressions for the torque, and for the longitudinal and transverse moments, reduce to

$$T = A_{11}^* \left[\left(\Phi_X^2 - K_Y K_T\right) \frac{\Phi_X l^5}{360} \right] + 4\left(D_{66}^* - \frac{B_{16}^{*2}}{A_{11}^*} \right) l \Phi_X, \tag{43}$$

$$M_l = A_{11}^* \left[\left(K_Y K_T - \Phi_X^2 \right) \frac{K_T l^5}{720} \right] + D_{11}^* l K_Y + D_{12}^* l \left(K_T - \frac{1}{R} \right), \tag{44}$$

$$M_T = A_{11}^* \left[\left(K_Y K_T - \Phi_X^2 \right) \frac{K_Y l^5}{720} \right] + D_{12}^* l K_Y + D_{22}^* l \left(K_T - \frac{1}{R} \right). \tag{45}$$

The reduced stiffness matrix for the $[+45°, -45°, 0°, +45°, -45°]$ layup is

$$\begin{pmatrix} N_x \\ M_x \\ M_y \\ M_{xy} \end{pmatrix} = \begin{bmatrix} 8.757 & 0 & 0 & 0.1361 \\ 0 & 0.819 & 0.616 & 0 \\ 0 & 0.616 & 0.799 & 0 \\ 0.1361 & 0 & 0 & 0.643 \end{bmatrix} \begin{pmatrix} \epsilon_x \\ \kappa_x \\ \kappa_y \\ \kappa_{xy} \end{pmatrix}. \tag{46}$$

The units for this matrix are: GPa mm for the top left-hand term (A_{11}^*), GPa mm^2 for the top right-hand 1×3 and (identically) for the bottom left-hand 3×1 matrix (B_{11}^*, B_{12}^*, B_{16}^*) and GPa mm^3 for the bottom right-hand 3×3 matrix ($[D^*]$).

Solving Eqs. (43)–(45) numerically allows equilibrium points ($T = M_l = M_T = 0$) in addition to the original state to be found for α greater than a critical value, which for this example is $\alpha \geqslant 56°$. Fig. 8 shows how the values of the strains at the equilibrium point vary with the initial cross-sectional angle α. A number of different solutions are possible, but only one is stable. The stable mode has $\Phi_X = 0$, and thus for this case a simpler model that neglects twist is adequate.

For large values of α, the stable solution tends towards $K_Y = 0.752/R$, $K_T = 0$, with $\Phi_X = 0$.

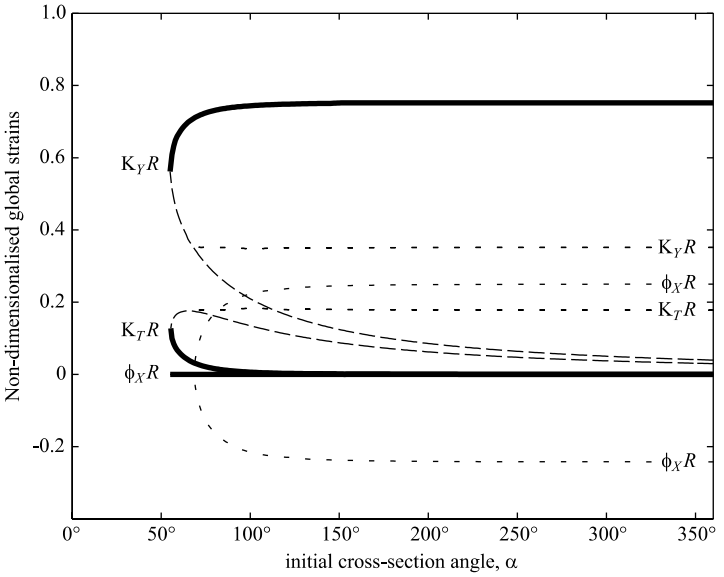

Fig. 8. Equilibrium points in addition to the initial state for the 45° antisymmetric layup. There is only one *stable* state, shown by the solid line, and this exists for $\alpha \geqslant 56°$. This solution has a corresponding unstable branch shown by the dashed line. At $\alpha = 69°$ a bifurcation leads to two additional twisted unstable solutions (one with positive twist, one with negative twist), shown by dotted lines.

3.2. Symmetric layup

For a symmetric layup, where $B^*_{16} = 0$, the expressions for the torque, and for the longitudinal and transverse moments, reduce to

$$T = A^*_{11}\left[\left(\Phi_X^2 - K_Y K_T\right)\frac{\Phi_X l^5}{360}\right] - 2D^*_{16} l K_Y - 2D^*_{26} l\left(K_T - \frac{1}{R}\right) + 4D^*_{66} l \Phi_X, \tag{47}$$

$$M_l = A^*_{11}\left[\left(K_Y K_T - \Phi_X^2\right)\frac{K_T l^5}{720}\right] + D^*_{11} l K_Y + D^*_{12} l\left(K_T - \frac{1}{R}\right) - 2D^*_{16} l \Phi_X, \tag{48}$$

$$M_T = A^*_{11}\left[\left(K_Y K_T - \Phi_X^2\right)\frac{K_Y l^5}{720}\right] + D^*_{12} l K_Y + D^*_{22} l\left(K_T - \frac{1}{R}\right) - 2D^*_{26} l \Phi_X. \tag{49}$$

3.2.1. 45° layup

The reduced stiffness matrix for the $[+45°, -45°, 0°, -45°, +45°]$ layup is

$$\begin{pmatrix} N_x \\ M_x \\ M_y \\ M_{xy} \end{pmatrix} = \begin{bmatrix} 8.757 & 0 & 0 & 0 \\ 0 & 0.868 & 0.665 & 0.345 \\ 0 & 0.665 & 0.848 & 0.345 \\ 0 & 0.345 & 0.345 & 0.681 \end{bmatrix} \begin{pmatrix} \epsilon_x \\ \kappa_x \\ \kappa_y \\ \kappa_{xy} \end{pmatrix}. \tag{50}$$

The units for this matrix are identical to those for the matrix in Eq. (46).

Solving Eqs. (47)–(49) numerically shows that there are the only stable solution in addition to the original state exists only for very large α. In the range of practical interest, e.g. $\alpha \leqslant 360°$, there are *no* additional stable solutions; unstable twisted solutions appear for $\alpha \geqslant 112°$. Fig. 9 shows how the values of the strains for the unstable equilibria vary with the initial cross-sectional angle α.

3.2.2. 40° layup

Although the additional stable solution for the symmetric 45° layup exists only for very large α, it would be wrong to conclude that this is always the case. Here we present a 40° layup that does have a second stable equilibrium solution for α in the range of practical interest.

The reduced stiffness matrix for the $[+40°, -40°, 0°, -40°, +40°]$ layup is

$$\begin{pmatrix} N_x \\ M_x \\ M_y \\ M_{xy} \end{pmatrix} = \begin{bmatrix} 9.844 & 0 & 0 & 0 \\ 0 & 1.092 & 0.647 & 0.398 \\ 0 & 0.647 & 0.660 & 0.281 \\ 0 & 0.398 & 0.281 & 0.663 \end{bmatrix} \begin{pmatrix} \epsilon_x \\ \kappa_x \\ \kappa_y \\ \kappa_{xy} \end{pmatrix}. \tag{51}$$

The units for this matrix are identical to those for the matrix in Eq. (46).

Solving Eqs. (47)–(49) numerically shows that, in addition to the original state, there is a stable twisted solution, that appears for $\alpha \geqslant 89°$, as well as the unstable solutions that are little altered from those presented in Fig. 9. Fig. 10 shows how the values of the strains at the equilibrium point vary with the initial cross-sectional angle α. Note that here, the stable state found is twisted, with $\Phi_X \neq 0$.

For large values of α, the stable solution tends towards $K_Y = 0.503/R$, $K_T = 0.018/R$, $\Phi_X = -0.095/R$.

3.3. Isotropic case

For the isotropic case, the expressions for the torque, and for the longitudinal and transverse moments, reduce to

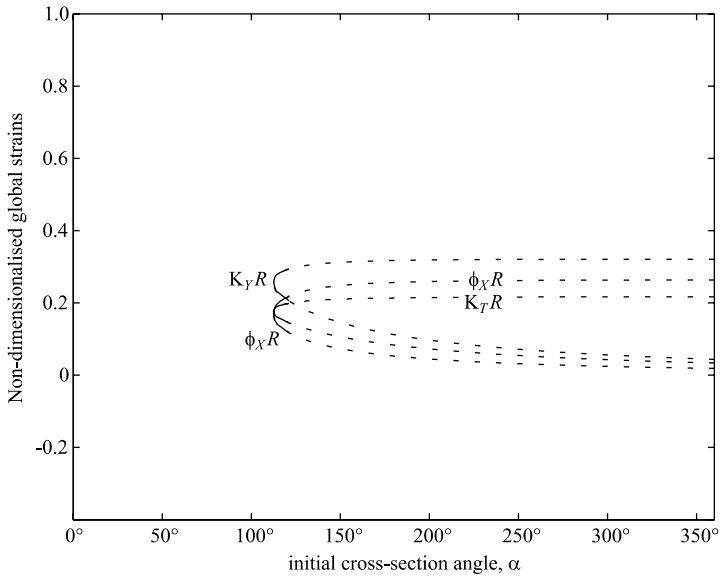

Fig. 9. Equilibrium points in addition to the initial state for the 45° symmetric layup. Unstable equilibria exist for $\alpha \geqslant 112°$, and are shown by dotted lines.

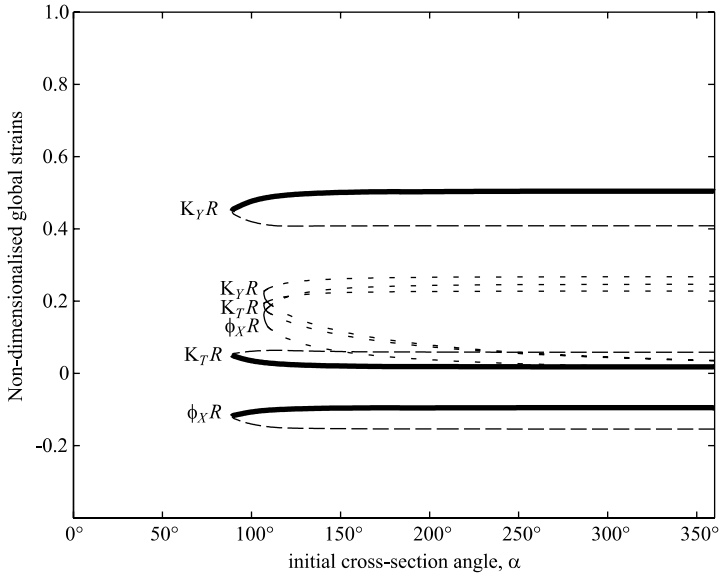

Fig. 10. Equilibrium points in addition to the initial state for the 40° symmetric layup. There is only one *stable* state, shown by the solid line, and this exists for $\alpha \geqslant 89°$. This solution has a corresponding unstable branch shown by the dashed line. Additional unstable solutions are shown by dotted lines.

$$T = Et\left[\left(\Phi_X^2 - K_Y K_T\right)\frac{\Phi_X l^5}{360}\right] + 2Dl(1-v)\Phi_X, \tag{52}$$

$$M_l = Et\left[\left(K_Y K_T - \Phi_X^2\right)\frac{K_T l^5}{720}\right] + DK_Y l + vDl\left(K_T - \frac{1}{R}\right), \tag{53}$$

$$M_T = Et\left[\left(K_Y K_T - \Phi_X^2\right)\frac{K_Y l^5}{720}\right] + vDK_Y l + Dl\left(K_T - \frac{1}{R}\right). \tag{54}$$

The reduced stiffness matrix of an isotropic sheet (Calladine, 1983, adjusted for the definition of κ_{xy}) is

$$\begin{pmatrix} N_x \\ M_x \\ M_y \\ M_{xy} \end{pmatrix} = \begin{bmatrix} Et & 0 & 0 & 0 \\ 0 & D & vD & 0 \\ 0 & vD & D & 0 \\ 0 & 0 & 0 & \frac{D(1-v)}{2} \end{bmatrix} \begin{pmatrix} \epsilon_x \\ \kappa_x \\ \kappa_y \\ \kappa_{xy} \end{pmatrix}, \tag{55}$$

where E is the Young's modulus of the material and v the Poisson's ratio, t is the thickness of the material, and $D = Et^3/12(1-v^2)$. For a 0.125 mm thick steel sheet this becomes

$$\begin{pmatrix} N_x \\ M_x \\ M_y \\ M_{xy} \end{pmatrix} = \begin{bmatrix} 25.875 & 0 & 0 & 0 \\ 0 & 0.0370 & 0.0111 & 0 \\ 0 & 0.0111 & 0.0370 & 0 \\ 0 & 0 & 0 & 0.0130 \end{bmatrix} \begin{pmatrix} \epsilon_x \\ \kappa_x \\ \kappa_y \\ \kappa_{xy} \end{pmatrix}. \tag{56}$$

The units for this matrix are identical to those for the matrix in Eq. (46).

Solving Eqs. (52)–(54) numerically shows that there are *no* stable solutions in this case. Fig. 11 shows how the values of the strains at the equilibrium point vary with the initial cross-sectional angle α. Unstable solutions appear for $\alpha \geqslant 62°$; for these solutions Φ_X is always zero. Because of this, a model that neglects

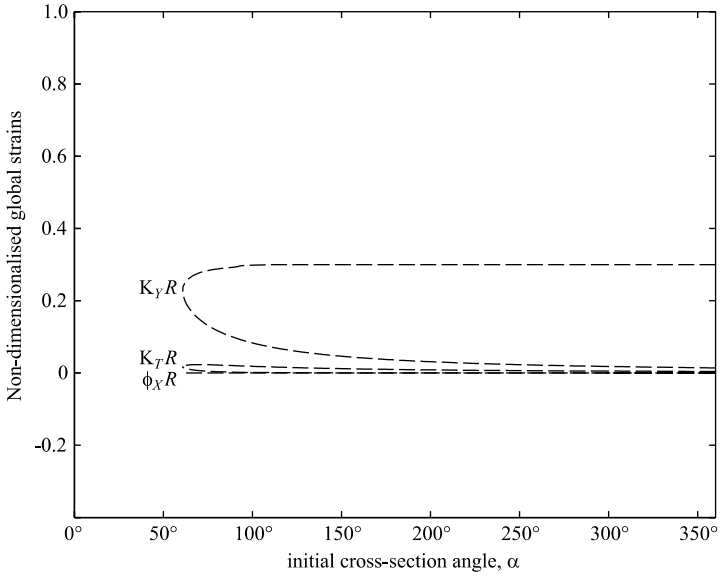

Fig. 11. Equilibrium points in addition to the initial state for the isotropic case. There are only unstable equilibria, which exist for $\alpha \geqslant 62°$, shown by dotted lines.

twisting would find this equilibrium point; however, it would not correctly predict the stability of the equilibrium, as the unstable mode of deformation involves twisting. These solutions correspond to the stable/unstable pair of solutions for the 45° antisymmetric layup, but in this case both branches are unstable.

4. Comparison with experimental results

For the 45° antisymmetric layup, the values given by the beam model for the longitudinal radius of curvature in the coiled state, $1/K_y$, can be compared with the results of experiments and finite element analyses reported by Iqbal et al. (2000). The finite element results presented were obtained by re-running Iqbal's analyses using the material properties given in this paper, which differ slightly from those used by Iqbal. The method is described in detail by Iqbal (2001), and a summary of the method will be given in Part II, where more detailed cross-sectional shapes are considered. The comparison is given in Table 1.

It can be seen from Table 1 that the results from the beam model correlate fairly well with the finite element results (particularly for large cross-sectional values of α), but less well with the experimental results. A possible reason for the disparity between the calculated and experimental results is that, at high strains, the matrix material is not linear elastic, but instead exhibits viscoelastic behaviour. The beam model presented in this paper, and finite element calculations, have all assumed linear elastic behaviour. If the disparity was due to viscoelastic effects, the beam model should correlate well with the *instantaneous* experimental radius at the moment of snap-through. The experimental measurements reported by Iqbal et al. (2000) were taken 24 h after snap-through. A brief experiment to try to capture an instantaneous radius was conducted; this measured a value of 37 mm, which accords much better with the calculated results.

The paucity of experimental data, and the poor agreement between the experimental and linear-elastic analytical and computational models, shows the need for further experimental and computational studies; work on this continues.

5. Conclusions

This paper has shown that modelling *twist* is essential to distinguishing between slit tubes that are bistable and those that are not. For many antisymmetric layups, twist is unimportant, and a model that neglects twist is adequate, but it will not be able to determine if the model is unstable in a twisting mode. For symmetric layups the second equilibrium point, if it exists, is twisted. For isotropic systems, a second equilibrium point exists that is not twisted, but it is unstable.

Table 1
The coiled longitudinal radius of curvature, $1/K_y$, found using the beam model, compared with experiments and finite element calculations for the antisymmetric 45° layup with $R = 29$ mm

α (°)	Experiment (mm)	Beam model (mm)	Finite element (mm)
280	30	38.5	39.6
200	30	38.5	40.5
120	32	38.7	43.0
90	33	39.2	45.7

The experimental results are taken from Iqbal et al. (2000) and the finite element results are found using the method described in Iqbal (2001).

Acknowledgements

We would like to thank RolaTube Technology Ltd., and particularly Andrew Daton-Lovett for help and support during this work. We would like to thank Sergio Pellegrino and Khuram Iqbal for many helpful discussions, and access to experimental and computational results. Diana Galletly was supported by a studentship from the EPSRC. Simon Guest acknowledges support from the Leverhulme Trust, and Harvard University Division of Engineering and Applied Sciences.

References

Calladine, C.R., 1983. Theory of Shell Structures. Cambridge University Press.

Galletly, D.A., 2001. Modelling the equilibrium and stability of slit tubes. PhD Thesis, University of Cambridge.

Galletly, D.A., Guest, S.D., 2004. Bistable composite slit tubes, II: A shell model. International Journal of Solids and Structures, this issue.

Halpin, J.C., 1984. Primer on Composite Materials: Analysis. Technomic Publishing Company.

Hull, D., 1981. An Introduction to Composite Materials. Cambridge University Press.

Iqbal, K., 2001. Mechanics of a bi-stable composite tube. PhD thesis, University of Cambridge.

Iqbal, K., Pellegrino, S., Daton-Lovett, A., 2000. Bi-stable composite slit tubes. In: Proceedings of IUTAM-IASS Symposium on Deployable Structures. Kluwer.

Kebadze, E., Guest, S.D., Pellegrino, S., in press. Bistable prestressed shell structures. International Journal of Solids and Structures. (in press), (doi:10.1016/j.ijsolstr.2004.01.028).

Rimrott, F.P.J., 1966. Storable tubular extendable members. Engineering Digest (September).

Seffen, K.A., Pellegrino, S., 1999. Deployment dynamics of tape-springs. Proceedings of the Royal Society of London A 455 (983), 1003–1048.

Timoshenko, S.P., Gere, J.M., 1961. Theory of Elastic Stability. McGraw-Hill, Inc.